JOURNAL OF SPACECRAFT AND ROCKETS
Vol. 29, No. 6, November–December 1992

Proposed Radiometric Measurement of the Wake of a Blunt Aerobrake

A. W. Strawa* and C. Park†
NASA Ames Research Center, Moffett Field, California 94035
and
W. C. Davy,‡ D. S. Babikian,‡ and D. K. Prabhu‡
Eloret Institute, Palo Alto, California 94303

This paper describes the aerothermal environment in the afterbody region of a blunt entry body. Recent ground-based experiments and computational predictions of the afterbody flow structure and radiation are presented. The similarity between the flowfield structures observed in the ground-based experiments and that obtained by calculation is encouraging. Approximate calculations of the radiative heating rate to the base are presented. Many of the phenomena associated with the expanding flow at the corner and the formation of the wake neck, however, are not well understood and require further study. A flight experiment is described that would use spectral and total measurements of the wake radiation as a nonintrusive diagnostic method to provide insight into the thermodynamic state of the wake gas.

Nomenclature

d = body diameter, m
p = pressure, N/m^2
q = radiative heat flux, W/cm^2
T = temperature, K
T_{tr} = translational and rotational temperatures, in nonequilibrium model
T_v = vibrational, electronic, and electron temperatures, in nonequilibrium model
V_∞ = flight speed, km/s
α = angle of attack measured from the normal to the base plane, Fig. 8
δ = wake neck viewing angle, Fig. 8
ϕ = shear-layer detachment angle, Fig. 8
ρ = density, kg/m3
τ = characteristic time constant for unsteadiness of the afterbody flow

Subscripts

b = base stagnation points
s = front stagnation point
0 = reference value in Eq. (3)

Introduction

THE concept of aeroassist has been evolving rapidly in the area of space transportation in recent years. In an aeroassist maneuver, a spacecraft enters Earth's atmosphere and utilizes the aerodynamic forces acting on the vehicle, to decelerate or change its course, and then exits the atmosphere to attain a desired orbit. As an alternative to consuming precious onboard fuel to perform an equivalent orbital transfer, the aeroassist maneuver effectively increases the available payload of space vehicles (see, e.g., Refs. 1–3). The vehicles performing such maneuvers have been named Aeroassisted Space Transfer Vehicles (ASTV). Proposed applications of this technique include transportation of communication satellites between geosynchronous Earth orbit (GEO) and low Earth orbit (LEO); on-site repair, refueling or resupplying of various satellites; and deceleration of vehicles entering planetary orbits or returning from the Moon or planets.

A conceptual ASTV, suited for the transportation of a communication satellite between GEO and LEO, is shown schematically in Fig. 1. A typical ASTV trajectory is shown in Fig. 2. The aerodynamic surface that produces the forces for the aeroassist maneuver is called the aerobrake. The payload is the assemblage of components behind the aerobrake consisting of the command and control module, astronauts' cabin, fuel tanks, rocket engines, and satellite cargo. It must be placed behind the aerobrake and shielded from the intense heat generated by the front shock layer and from the convective and radiative heating environment produced by the wake.

The technology associated with aeroassist has been identified as an enabling technology for the nation's space transportation efforts.[4,5] In addition to computational and ground-

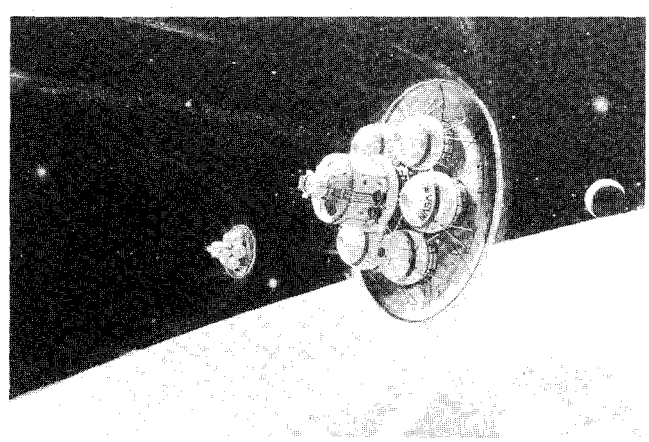

Fig. 1 Artist's sketch of an ASTV concept.

Presented as Paper 91-1408 at the AIAA 26th Thermophysics Conference, Honolulu, HI, June 24–26, 1991; received Jan. 11, 1992; revision received April 1, 1992; accepted for publication May 8, 1992.

*Research Scientist. Senior Member AIAA.
†Head, Experimental Aerotherodynamics Section. Associate Fellow AIAA.
‡Research Scientist. Member AIAA.

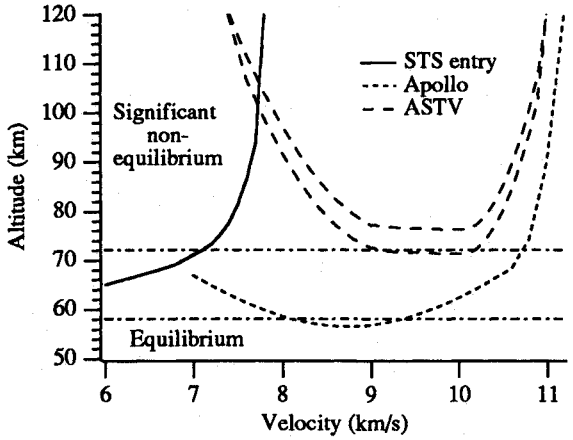

Fig. 2 Trajectories of ASTV and other flight vehicles.

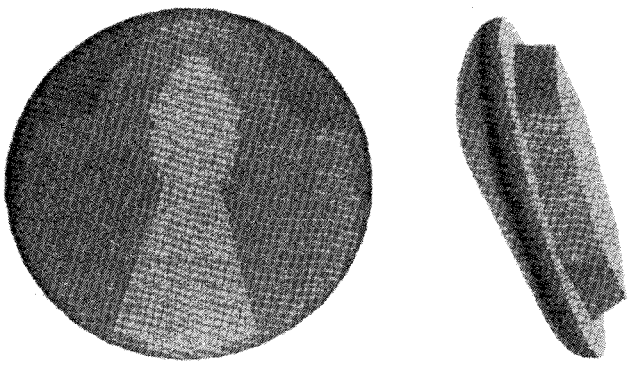

Fig. 3 Planform and profile of the AFE vehicle.

based experiments designed to study aeroassist technology, the Aeroassist Flight Experiment (AFE) has been conceived and pursued by NASA. The AFE vehicle is approximately a ¼-scale model of a typical ASTV. Figure 3 shows the profile and planform of the AFE. The latest mean trajectory would have it enter the atmosphere at a velocity of about 9.9 km/s, and reach a perigee altitude of about 75 km. The AFE program was cancelled recently due to budgetary constraints. Nevertheless, aeroassist remains an important and promising technology for the nation's space effort and warrants further study.

One aspect of particular interest in ASTV research is analysis of the wake flow. The afterbody assemblage must be protected from the convective and radiative heating environment produced by the wake flow. Prediction of this environment must, therefore, be of sufficient accuracy to adequately design the thermal protection for the payload. Although convective heating rates on the base are generally small,[6] very high localized heating rates can occur if the shear layer separating from the frustum, or corner, of the vehicle impinges on the afterbody. At such an impingement point, the convective heat transfer rate can be of the same order as that experienced at the front stagnation point.[7] Also previous experimental work suggests that the radiative heating to the afterbody could be as high as 5% of that at the forebody stagnation point.[8]

The wake flowfield influences the shear-layer turning angle, the convective and radiative heat flux to the payload, and to some degree, vehicle aerodynamics. An approach in studying ASTV wake flows is to use the radiation inherent in the corner and wake flows as a nonintrusive diagnostic means to gain insight into the thermodynamics of the flowfield. Such an experiment, which is designed to study wake phenomena of the proposed AFE, is called the Afterbody Radiation Experiment (ARE). The objectives of this paper are to state the importance and complexity of ASTV wake flows, to justify the ARE, and to briefly describe the proposed instrumentation.

Wake Flow Characteristics

Only a brief description of wake flow phenomena will be presented in this paper, however, an excellent review of hypersonic wake flows was given in 1965 by Lykoudis.[9] During this discussion, it will be helpful to refer to the sketch in Fig. 4 which shows the dominant features and physical phenomena important in the ASTV flowfield. Figure 5 is a shadowgraph of an AFE model that has recently been obtained in the Ames ballistic range.[10] The velocity of the model was 5 km/s, the Reynolds number (based on a model diameter of 2 cm) was 600,000, and the angle of attack was about 10 deg nose down. The forebody shock, shear layers, neck region, and recompression shocks that are shown schematically in Fig. 4 can be seen in the shadowgraph.

Evidence of Wake Radiation

The possibility that there may be radiation in the afterbody region of a re-entry body at high entry speeds was first considered for the Apollo program. Canning and Page measured spectral radiation from the stagnation and wake regions of ablating and nonablating models flying at a speed of 6 km/s.[11] The largest amount of radiation from the wake of the nonablating model was observed to be between wavelengths of 200 and 600 nm. (Their instrument was not sensitive to wavelengths below 200 nm.) In 1965, Stephenson[12] launched axisymmetric blunt body models in a ballistic range at flight speeds up to 10 km/s. The models were made of plastic materials that ablated during the flight. The hot gas and ablation products emitted strong radiation both in the forebody and in the wake regions. A photograph of the luminous flowfield taken from Stephenson is shown in Fig. 6a. The observed radiation was due predominantly to CN, a product of the ablation process. The area from which the strongest radiation occurred for the nonablating case was similar to this ablating case and the figure serves to illustrate some of the predominant flow features. There is evidence of strong radiation in the wake, particularly in the region of the wake neck, located about one body diameter aft of the model. The photograph also shows bright and dim features in the luminous wake and structure reminiscent of vortex shedding which are indicative of unsteadiness.

Prior to the Apollo missions, a flight experiment of a ⅓-scale model of the Apollo vehicle, named Fire, was flown at a speed of 11.3 km/s to study the radiative heating phenomena on both the forebody and the afterbody regions. The Fire

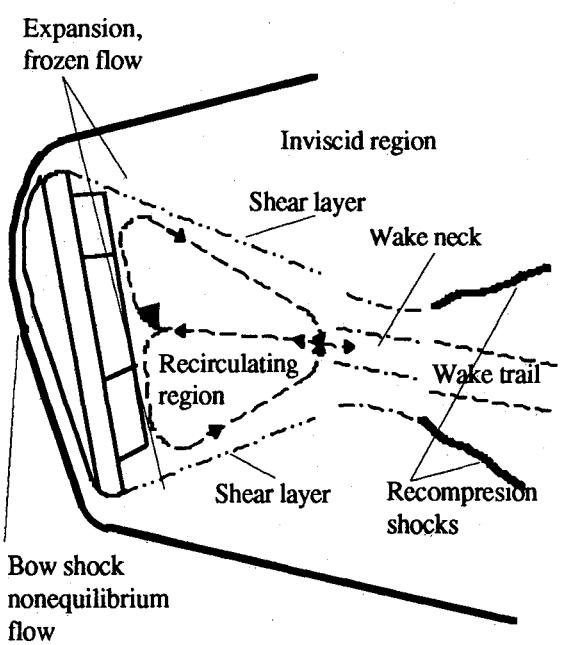

Fig. 4 Physical phenomena important to ASTV.

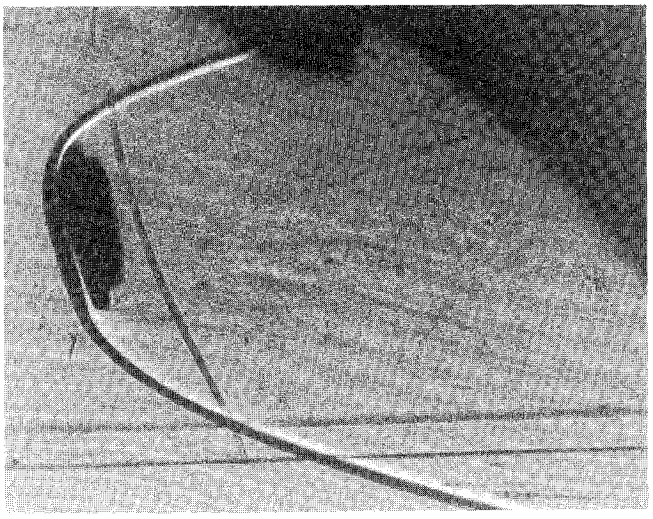

Fig. 5 Shadowgraph of AFE model flying in Ames's ballistic range at 5 km/s with $Re = 600{,}000$.

vehicle, like the Apollo vehicle, was axially symmetric. But its center of gravity was offset so that it would attain a nonzero trim angle of attack. As a result, the flowfield around the vehicle was three dimensional and produced substantial lift. The heat shield was designed such that there would be no ablation, at least while the measurements were being made. A radiometer was placed to view the expanding region of the flowfield behind the heat shield. Since the vehicle rolled, the radiative flux was measured at all possible azimuthal angles. The measured radiative flux was highest at the extreme leeside, and was determined by Cauchon[13] to be equal to 5.3% of that at the forebody stagnation-point. Peak radiative heating on the afterbody was observed to occur prior to peak radiative heating at the front stagnation-point.

In the 1970s, measurements of the radiative flux on the base region of a nonablating Galileo entry probe were made by Shirai and Park[14,15] in a shock tube at $M = 1.5$. They measured radiative flux to the base to be about 4% of that at the front stagnation point. Figure 6b shows a scale model of the Galileo probe made of a graphite material that was flown in krypton in a ballistic range at a flow Mach number of 20. The picture was taken at a point in the range close to the launcher where ablation had not yet occurred. Here, peak luminosity occurred at a distance of about one body diameter downstream.

Wake Radiation for the AFE

Even though the existing experimental data mentioned above show the radiative flux incident on the base can be as high as 5% of the front stagnation-point radiation, the radiation to the base of the AFE may be substantially different. The differences are the scale of the AFE and the pressures of the overall flowfields. The Fire vehicle was much smaller than AFE and the peak radiative heating did occur at an altitude much lower than that expected for the AFE; the wake flow at that altitude was almost certainly in equilibrium. The Fire vehicle had a conical afterbody which likely prevented separated flow from occurring in the region where the base radiation sensor was located, whereas separation would certainly occur at the corners of the AFE vehicle. The experiments conducted on the Galileo entry model were made using monatomic gases at a high pressure (the stagnation-point pressure was greater than 20 atm) and, therefore, the afterbody flow was likely to have been in thermochemical equilibrium. Throughout the flight regime of the AFE, the corner flow is expected to be in a nonequilibrium state, while the wake neck may be at equilibrium. The extent of nonequilibrium flow significantly effects the resulting radiation as described below.

To facilitate the design of the ARE experiment, the anticipated range of the radiative flux incident on the base, the location of the principal luminous sources, and the spectral distribution of the radiation must be known. Past experimental data cannot be relied upon to predict these quantities, nor can current ground-based facilities appropriately simulate the AFE flowfield. Therefore, ground-based data and existing flight data must be used only to verify computational solutions which then can be extrapolated to the proper conditions for AFE. To this end, experiments and calculations have been performed to estimate the required quantities.

In past experiments, significant gas luminosity occurred in two regions of the afterbody flow: the expanding region at the shoulder and the wake neck. However, the physical conditions that would cause the radiation for the case of the AFE in these regions would likely be very different. In the expanding region, the flow would be supersonic, the translational temperature and pressure would be fairly low, and the density would be high. However, the gas would likely be in thermochemical nonequilibrium and the internal energy states would be highly excited, causing the energetic atoms and molecules to radiate. Therefore, in order to accurately predict the radiation in this region for the AFE, it is essential to have an accurate thermochemical model to predict the state of the gas correctly.

The neck region would likely radiate because the pressure and temperature would be high and the flow subsonic. If the wake flow were steady, there would be a saddle point in the neck region where the flow velocity would approach zero. Chapman[16] and Korst[17] showed that the upper limit to the neck pressure for supersonic flow past blunt bodies was a substantial 25% of that at the front stagnation point. At this point, all of the energy of the flow was in the internal energy and thermal modes, and hence the translational temperature was high. If the internal modes were in equilibrium with the translational temperature, substantial radiation would occur. Park[18] used a one-dimensional model of the wake flowfield of the Galileo probe and a nonequilibrium radiative transfer model and found that the ratio of base to stagnation-point radiative flux, q_b/q_s, was proportional to the square of the ratio of the base pressure to the front stagnation-point pressure, p_b/p_s,

$$\frac{q_b}{q_s} \sim \left(\frac{p_b}{p_s}\right)^2 \tag{1}$$

This proportionality is expected to hold for the AFE case despite the difference in freestream pressure. Therefore, it is essential to have a fluid mechanical model that correctly pre-

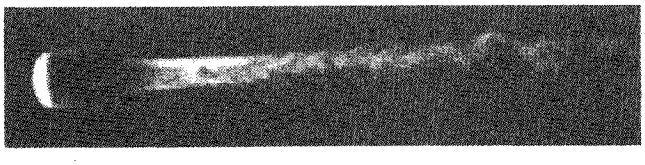

a) luminous blunt body in air, ballistic range, M = 30, Stephenson[12]

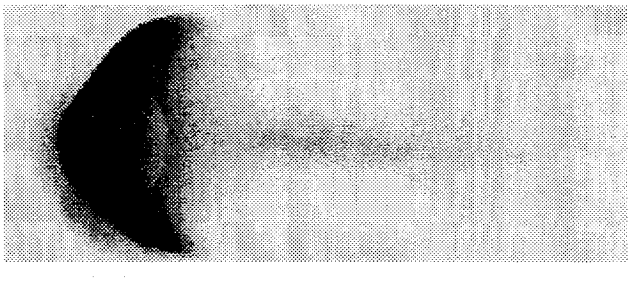

b) Galileo probe in krypton, ballistic range, M = 20.

Fig. 6 Evidence of wake radiation: a) luminous blunt body in air, ballistic range, $V = 10$ km/s, Stephenson[12]; and b) Galileo probe in krypton, ballistic range, $M = 20$, Park.

dicts the base and neck pressures in order to predict the radiation in this region.

Importance of the Shear Layer

Prediction of radiation in both the expansion and wake neck regions requires knowledge of the flowfield and the thermochemical nonequilibrium phenomena therein. In general, the base flowfield is critically dependent on the shear layer phenomena. The shear layer is the border between the supersonic inviscid flow and the viscous recirculating flow. Across the layer, the tangential momentum of the supersonic flow is transmitted to the recirculating flow. The amount of momentum transferred determines the velocity inside the layer, which in turn determines the pressure at the neck saddle point where the velocity is recovered as pressure. The transfer of momentum is different for laminar and turbulent flow. A laminar shear layer imparts only a small amount of tangential momentum into the recirculating flow. This leads to a low neck pressure and weak neck radiation. In contrast, a turbulent shear layer imparts a large amount of momentum and leads to a large neck pressure and radiation.

For the AFE, the shear layer would originate at the edge of the heat shield, where it would inherit a velocity distribution from the boundary layer over the forebody. According to various calculations performed in recent years, the boundary-layer flow over the forebody is expected to be laminar at the heat shield edge. Laminar shear layers have, approximately, a linear variation in properties across the layer, and are fairly thick in order to impart a momentum of meaningful magnitude. On the other hand, the shear layers observed experimentally, see for example Fig. 5, were quite thin, and are interpreted to be a sign of turbulent flow. In turbulent flow, a large transverse gradient in flow properties occurs at the middle of the shear layer, with a more gradual variation further from the shear layer. The large transverse gradient in flow properties in the middle of the layer will produce the thin appearance of the layer seen in the shadowgraph, while the gradual variation makes it possible to impart a large amount of tangential momentum. Thus, it seems that the shear layer underwent a laminar-to-turbulent transition between the heat shield edge and the neck. The point of transition must be predicted accurately to obtain the proper wake properties for the AFE.

Besides affecting the base and neck pressure, the shear layer is important for another reason, namely the possibility of impingement on the afterbody. The AFE project estimated the convective heating due to shear-layer impingement for the AFE at 20.7% of the stagnation-point convective heating.[19] Using a chemically reacting Navier-Stokes code, Gnoffo et al.[20] estimated the convective heating due to shear-layer impingement to be 13% of the stagnation value. However, experiments have shown that heating rates are highly dependent on shear angle and can be of the same order as that at the stagnation point.[7] Thus, it is important to predict reliably the angle through which the shear layer turns and the magnitude of the convective heating it causes. The intrinsic shear-layer turning angle, defined as the angle between the shear layer and the direction of the mean flow in the base region, should be a function only of the ratio of the base pressure to the front stagnation-point pressure because it must be the Prandtl-Meyer turning angle corresponding to that pressure ratio.

Experiments measuring the shear turning angle for the AFE vehicle have been conducted by Wells[21] in a wind tunnel and by Strawa et al.[10] in a ballistic range. The ballistic range tests were conducted with AFE models 2 cm in diameter flown in air at 5 km/s and at freestream Reynolds numbers of about 600,000 based on model diameter. The convention used for the angles are defined in Fig. 7. The angle of attack α was measured from the relative velocity vector with positive angles nose up. The shear-layer detachment angle ϕ was measured from the vehicle base to the shear layer as measured in the shadowgraphs. Angle ϕ is geometrically related to the shear-layer turning angle mentioned earlier.

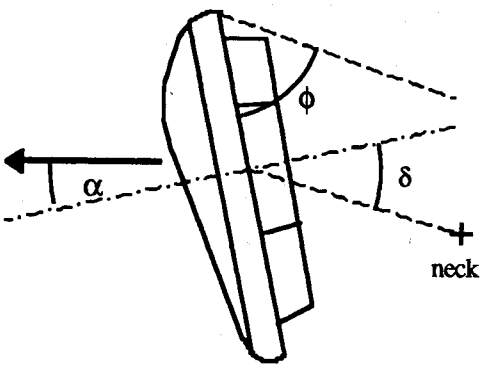

Fig. 7 Diagram showing ballistic range measurement angles.

The shear-layer detachment angle at the upper corner is plotted in Fig. 8 as a function of angle of attack. The shear layer at the upper corner is most likely to impinge on the afterbody. Of the many shadowgraphs taken during the range tests, only those which exhibited small degrees of yaw and roll are plotted. The uncertainty in the measurements was about ± 1 deg due to the reading errors. Shear-layer impingement occurred for $\phi < 46.4$ deg.

The AFE vehicle is designed to trim at $\alpha = -17$ deg and the vehicle would be kept within trim $\alpha \pm 5$ deg for most of the flight. At $\alpha = -17$ deg, the range data showed the shear layer detachment angle to be about $\phi = 50$ deg; at an angle of attack of $\alpha = -22$ deg, the shear-layer detachment angle was $\phi = 45$ deg. These values are comparable with the $\phi = 50$ deg value obtained by Wells in his wind-tunnel experiment. Thus, it is likely that the shear layer from the upper corner would impinge on the afterbody during some portion of the AFE flight.

The scatter of the data in Fig. 8 was quite large, about ± 5 deg. This scatter was interpreted to be due to fluctuations in the base pressure due to unsteadiness in the flowfield. The unsteadiness of the flow can be deduced from another distinct feature in the shadowgraph in Fig. 7: the waviness of the recompression shock. The photographs of Stephenson,[12] Fig. 6a, and of Park, Fig. 6b, also exhibit this wavy characteristic. The characteristic time scale of the unsteadiness τ can be estimated from the wavelength of the oscillations in the recompression shock and the vehicle velocity as

$$\tau = \frac{d}{V_\infty} \tag{2}$$

For the AFE vehicle, the implied frequency would be between about 1 and 5 kHz. Another important feature of the afterbody region for instrument design is the wake neck viewing angle δ defined as the angle from the center of the base of the vehicle to the center of the neck region (see Fig. 7). The neck viewing angle was measured from the shadowgraphs taken in the ballistic range.[10] The tests shown here were conducted at two velocities, 2 and 5 km/s. The data show a dramatic effect of angle of attack on the neck viewing angle: at an angle of attack of about 5 deg the neck viewing angle was nearly zero, but increased markedly as the angle of attack increased or decreased. The behavior was the same at velocities of 2 and 5 km/s. If a reliable prediction of the afterbody flow phenomena is to be achieved for the AFE at flight conditions, the laminar-to-turbulent transition behavior, the shear-layer detachment angle, the neck viewing angle, and the unsteady nature of the flow must be correctly characterized.

Computational Modeling and Results

For the design of the ARE experiment, the anticipated range of the radiative flux incident on the base, the location of the principal luminous sources, and the spectral distribution of the radiation must be known. The methods that were used to determine these parameters are discussed next.

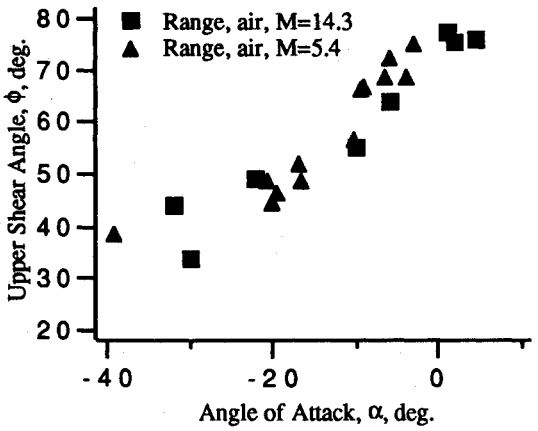

Fig. 8 Shear-layer angle vs angle of attack.[10]

Flowfield Calculations

Gnoffo and Greene[22] made perfect-gas calculations in the AFE wake that showed weak shock impingement on the upper shoulder of the instrument shroud at trim ($\alpha = -17$ deg). Their grid in the wake region was coarse and no evidence of wake neck structure was seen. Li and Wey[23] made calculations with a chemically reacting code for the AFE wake, but their grid in the wake also was coarse and the solution did not show wake structure. Later, Gnoffo et al.[24,20] made calculations for the near wake of the AFE with a nonequilibrium chemistry code. Their calculations showed shear layers and indicated a diffuse neck region with velocity contours converging at about 3 body diameters downstream, the extent of their computational zone. Palmer[25] made similar calculations of the AFE flowfield including nonequilibrium chemistry. However, his calculations were limited to the wake flow immediately behind the base. Tam and Li[26] made a comparison of the flow structure, temperature, and species concentrations computed from these methods. They found significant differences in the results on the vehicle surface, across the shock layer, and behind the base. The level of detail in the wake structure that is required here was not provided by any of the solutions. Computations which include nonequilibrium chemistry require a large amount of computer time. For example, Palmer's code required approximately 50 h of CPU on a Cray II computer to reach a converged solution.

These previous calculations were not suitable for present purposes. A large portion of the radiation from the wake is expected to come from the neck region and possibly from the recompression shocks that form after the neck. These structures, clearly evident in ballistic range shadowgraphs, were not clearly seen in the computations. To design an experiment aimed at measuring the radiation from the wake it is necessary to know the location of the wake neck and the formation of the recompression shock at trim and off-trim attitudes. Wake structure is primarily a fluid dynamic phenomenon. The effects of chemistry should have only second-order effects on this structure, as confirmed in the parametric studies of Gnoffo et al.[20] The expanding flow would quickly freeze, thermochemically, past the shoulder. An ideal-gas code (γ not equal to 1.4) with an adaptive grid was used to model the flow in the afterbody out to about 4 body diameters downstream. Computations were carried out in two steps: the flowfields were computed using codes that model the fluid mechanics and thermochemistry; the radiation field was then computed using radiation models. This section briefly describes the models and summarizes their results. Palmer's[25] nonequilibrium solution at the shoulder of the vehicle was used as the inflow boundary for the ideal-gas solution. The gas model was for air, consisting of 11 species including electrons and used Park's[27] modification of the Landau-Teller model to represent the thermal nonequilibrium phenomena. An adaptive grid code, developed by Davies and Venkatapathy,[28] was used to sharpen the flow features. Calculations were performed at five angles of attack. Details of the technique can be found in Ref. 29.

Temperature contours in the pitch plane of the AFE, computed using the method outlined above, are shown in Fig. 9. The angle of attack was $\alpha = -17$ deg (AFE trim angle of attack) and the flight conditions were for an altitude of 77.9 km and a velocity of 8.9 km/s. Flow features that can be seen in the figure, such as shear layers and recompression shocks, were similar to those observed in the ballistic range shadowgraph in Fig. 5. The shear-layer detachment angle and location of the neck have been determined using the same methods and conventions used in obtaining the experimental values presented in Fig. 8.

The calculated shear-layer detachment angle, measured from Fig. 9, at the upper edge of the vehicle was $\delta = 62$ deg, which was somewhat larger than the experimental value about $\delta = 50$ deg, but qualitatively the agreement appears quite good. The location of the wake neck, noted on the figure, was identified by a neck viewing angle of $\phi = 18$ deg down from the vehicle centerline and is located 1.1 body diameters aft. The experimental values for the location of the neck are 25 deg down and 1.0 body diameters aft, given in Ref. 10. Although these features did not coincide exactly with those of the experiment, the results indicated that progress is being made in our ability to model the afterbody flow region of the AFE.

Radiation Calculations at the Shoulder

The flow calculated at the shoulder was in a state of thermochemically nonequilibrium. To calculate the radiative flux at the shoulder, Palmer's[26] flowfield solution was used for species concentrations and temperatures. The radiation was calculated using NEQAIR[30], assuming a quasisteady state (QSS) population distribution in the electronic states, i.e., the time rate of change of number density in an electronic state is much less than the difference of the rates populating and depopulating that state. This step allowed NEQAIR to calculate a separate electronic temperature for each electronic state, providing a multitemperature radiation model. As program input, NEQAIR required species concentrations and two temperatures at each point in the flowfield; namely T_{tr}, representing the atomic and molecular translational and the rotational temperature and T_v, representing the electron translational and the vibrational temperature.

The spectral distribution of the radiative flux (measured in units of W/cm^2-sr-μ) incident on the AFE surface along a line of sight extending from the upper instrument shroud parallel to the back plane and in the plane of symmetry is shown in Fig.10. The spectrum was plotted from 200 to 1000 nm with a resolution of about 0.6 nm, which was the approximate reso-

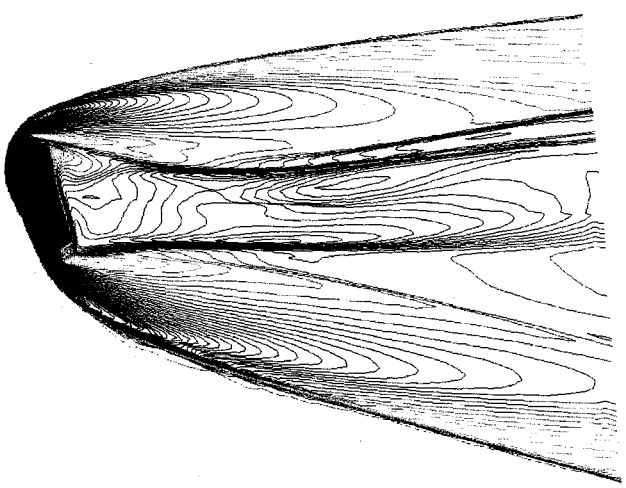

Fig. 9 Temperature contours of AFE flowfield-pitch plane.

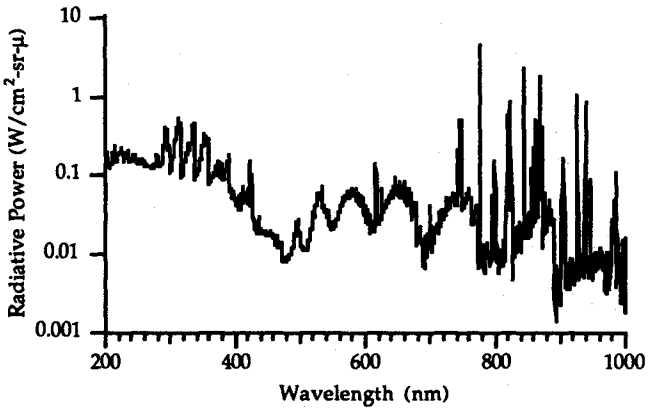

Fig. 10 Computed spectra at the upper shoulder line of sight for the AFE.

lution expected in the ARE spectrometers, although, the spectrum was computed from 190 to 1400 nm. The continuum radiation from the vacuum ultraviolet below 200 nm decreased rapidly. Separate calculation of the contribution of line radiation from N, N^+, O, O^+, $N_2(1-)$, $N_2(2+)$, $N_2(1+)$, $NO\beta$, $NO\gamma$, and O_2(Schumann-Runge) showed that this contribution was not significant. Note that the spectral power varied over nearly four orders of magnitude. One of the proposed ARE instruments is a radiometer that integrates the total radiation from 200 to 1400 nm. The radiative flux along this line of sight from 200 to 1400 nm was computed to be 8×10^{-3} W/cm^2-sr.

Radiation Calculations at the Base

The other major source of radiation in the wake is the neck. The flow in the wake would likely be in thermodynamic equilibrium. It was reasonable, then, to use the flowfield calculated with an ideal gas code and use an engineering correlation to obtain the corresponding radiation. The engineering correlation, based on thermodynamic equilibrium, was developed by Nardone et al.[31] This correlation, which must be used for applications that are reasonably similar, relates the radiative emission at a point (W/cm^3) to the local density and temperature by the equation

$$E=\epsilon\left(\frac{\rho}{\rho_0}\right)\left(\frac{T}{T_0}\right)^n \tag{3}$$

where ϵ and n are constants, which must be found by comparison with experimental data, or theoretical results.This correlation was used to calculate the radiative emission for the ideal-gas solution mentioned above, throughout the base region of the AFE vehicle, using $\epsilon=7\times10^{-15}$ W/cm^3 and $n=17.25$. The exponential factor of 17.25 would make the absolute magnitude of radiation very sensitive to the temperature chosen. However, of interest here is the location of the most intense radiating regions of the flow, not their absolute magnitudes. The emission contour plot in the pitch plane is shown in Fig. 11. The regions of peak intensity are indicated and are seen to correspond to the regions of high temperature shown in Fig. 9.

The directional intensity distribution was calculated from the emission values given by Eq. (3) by solving the equation of radiative transport along a line of sight generated from a point on the surface. This distribution is also plotted in Fig. 11 as the solid curve representing the logarithm of the relative intensities along the lines of sight from the detector position. The intensity lobe at $\theta=30$ deg in the lower half-pitch plane corresponds to the high-intensity neck region in the lower half of the wake. Plots such as this are very useful in determining the proper placement, field of view, and orientation of the ARE instruments. The radiative heating, integrated over the 90- deg field of view shown in Fig. 11 was 0.26 W/cm2. As mentioned previously, this value was very sensitive to the temperature distribution in the flowfield.

Discussion

The computational results presented in the previous section are encouraging. They show that significant progress is being made in understanding the wake region. Calculated features of the wake flowfield, including the shear layer, the location of the neck region, and formation of recompression shocks were generated and were in qualitative agreement with available experimental data. But significant differences did exist between the computed results and the experimental results.

The calculated shear-layer detachment angle ϕ was larger than that measured and the calculated neck location was closer to the body centerline than measured. The minimum point in the wake velocity field occurred at about the point where the neck was observed experimentally, but, the local maxima of temperature, pressure, and density did not occur at the same location. Experimental measurement of these quantities is very difficult, but are crucial for a better understanding of hypersonic wakes.

The two-temperature thermochemical model and the QSS approximation in NEQAIR were developed to account for the observed radiation and shock standoff distance measured in shock tubes or in the shock layer behind a strong bow shock wave. A new model for expanding flows may be necessary and may be considerably different from the compressive flow model. For example, the present model first solves the chemistry, transport and flow equations using Park's two-temperature model,[27] which, among many other assumptions, equates the electronic, electron kinetic, and vibrational temperatures, and also assumes that all of the reactions take place in the ground state. After the chemistry portion of the calculation is completed, the total population of each species is then partitioned between the electronic states by the QSS approximation method. This separation of the chemistry portion of the code from the excitation portion greatly simplifies the computational task. In expanding flows, the radiant intensity appears to be strongly related to the vibrational temperature, which means that the effective electronic temperature is strongly coupled to the vibrational temperature. Furthermore, the vibrational temperature is strongly coupled to the kinetic temperature of the free electrons, which play a major role in the electronic excitation process. Thus, in expanding flows it is possible that the chemistry and excitation processes are closely coupled and cannot be separated.

In the nonequilibrium flow at the shoulder, the low pressure and density in the wake resulted in a low collision rate among the gaseous species. Thus, the population of the excited states

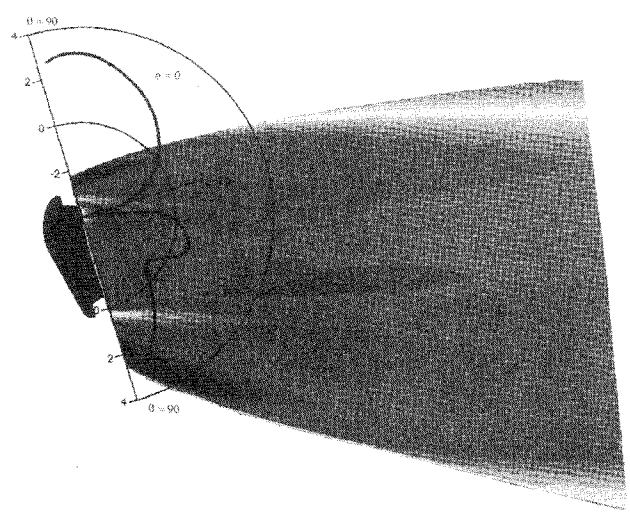

Fig. 11 Radiative power contours and polar plot of the normal intensity in the pitch plane of the AFE.

was lower, possibly very much lower, than the Boltzmann population because of radiative quenching. To examine the effect of the QSS approximation on the calculated radiation incident on the upper shoulder point, calculations were made replacing the QSS code with a simple Boltzmann distribution using the electronic temperature (which is equal to the vibrational temperature) found in the chemistry portion of the solution. The radiative flux along the line of sight shown in Fig. 10, calculated using NEQAIR and Palmer's flowfield solution[26] and integrated over the line of sight and from 200 to 1000 nm, was $6.8 \times 10\text{-}2$ W/cm2-sr. Comparing this with the 0.8×10^{-2} W/cm^2-sr calculated using the QSS approximation shows that the collision rates in the flowfield, used by the QSS code, were not adequate to maintain a Boltzmann population in the upper states. If they were, the radiation flux incident on the surface for this line of sight would be higher by nearly a factor of ten.

The final point of discussion is the effect of unsteadiness in the wake region. In the sketch of the hypersonic wake shown in Fig. 4, the location of the center of the neck is defined as a saddle point where the velocity goes to zero. Here, the pressure, density, temperature, and radiation are expected to be a maximum. The coincidence of these features did occur in a steady, ideal-gas calculation made for a two-dimensional half-cylinder by Venkatapathy et al.[29] A real, three-dimensional wake flow, such as that for the AFE, however, would be unsteady and much more complex. The flow in the neck region would, in fact, never actually come to rest with respect to the vehicle. In an unsteady flow, the kinetic energy contained in the flowfield would be larger than that in a steady flow because of the additional, and rapidly varying, velocity component. Thus, a smaller fraction of the total energy of the flow would be available to excite the internal energy states of the gas. The resulting temperatures, and hence the radiation intensity, could be noticeably reduced, but the amount of the effect is presently unknown. Although the existing experimental evidence indicates that the base flowfield was unsteady, all theoretical calculations performed to date assume that the flow was steady.

There is much uncertainty both in the thermochemical and radiation models used in calculating hypersonic wake flows. Although progress in understanding the principal features and some of the details of wake flows has been made by both laboratory and theoretical research, the uncertainties cannot easily be sorted out with ground-based testing alone since ground-based facilities cannot attain the combination of flight velocity, enthalpy, and vehicle size needed to properly simulate the thermochemistry of the ASTV flowfield. Therefore, the ARE was included as one of the experiments to be flown aboard the AFE. The objective of the ARE was to measure the radiative flux to the afterbody and use the radiation inherent in the wake flowfield as a nonintrusive diagnostic method to learn about the thermodynamic state of the wake gas. This data, together with that of other experiments and computational modeling, would increase understanding of hypersonic wake physics and lead to more efficient ASTV designs.

Proposed Instruments

The proposed ARE is composed of two kinds of optical instruments: the Total Radiation Detector (TRD) and the High Resolution Spectrometer (HRS). The TRD is a thermopile that would measure integrated spectral energy from 200 to 2600 nm, and the HRS is a spectrometer with a spectral range of 200–770 nm and a spectral resolution of about 0.6 nm. Each instrument would look through a sapphire window to record the radiative flux from the flowfield falling on the detectors. Data would be recorded once every 3 s during the aeropass.

The dynamic range of the HRS is 10^7. This is because a dynamic range of 10^4 is required to capture the features within the spectra at any instant along the trajectory, as seen from Fig. 10, and 10^3 to ensure that the signal is detected throughout the aeropass.

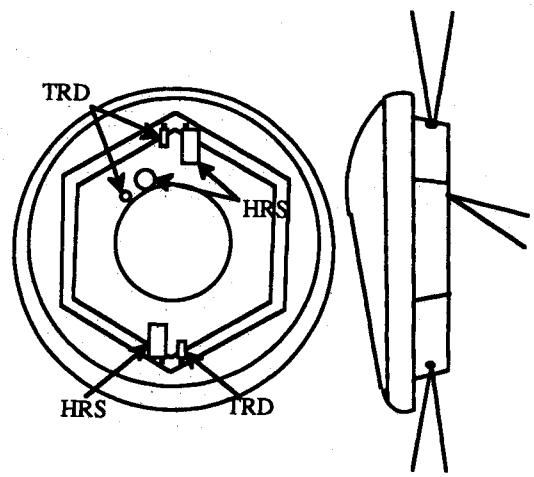

Fig. 12 ARE instruments location and fields of view.

The locations of the three TRDs and three HRSs that comprise the ARE suite of instruments are shown in Fig. 12. The radiation emitted by the flow as it expands over the frustum at the top and bottom of the vehicle would be measured by separate TRDs and HRSs. Because of the three-dimensional nature of the AFE forebody, the state of the fluid expanding about the frustum at the bottom of the vehicle would be quite different from that at the top of the vehicle. This data would be very valuable in corroborating the thermochemical model in the expanding flow region and ensuring that the interaction between the fluid mechanics and chemistry is properly handled.

The base radiation would be measured by a TRD and an HRS located at the base of the afterbody and pointed at the wake neck. The aft looking instruments would be canted down 25 deg from the vehicle centerline to observe the wake neck at its most probable location, as determined from the aforementioned ballistic range experiments.

The variation of radiation intensity with altitude and velocity would be expected to have a very low frequency, much less than 1/6 Hz. Variations of the intensity due to spacecraft motions would be expected between 1/2 and 1 Hz. Higher-frequency variations in the intensity could be caused by fluid mechanical instabilities and turbulence in the afterbody flow and, as mentioned earlier, would likely be at frequencies greater than 1 kHz. These variations would be filtered out of the data electronically.

Conclusions

Radiative and convective heating to the afterbody of an ASTV could be large enough to necessitate some sort of thermal protection for the afterbody. Large convective heating rates would be expected if the shear layer, separating from the vehicle corner, impinged on the afterbody. Estimates presented here suggest that the radiative flux to the afterbody may be as high as 5% of the front stagnation point. However, there are many differences between the experiments conducted to date, and any future flight experiment or a full-scale ASTV, that will make current measurements of the shear layer and radiation difficult to apply directly to full-scale vehicles. Many of the phenomena associated with the wake flows are not well understood at present. These include the energy exchange mechanisms in an expanding corner flow, radiation mechanisms in the wake, and turbulence and unsteadiness in the shear layer and wake. To accurately predict the wake flow of an ASTV and radiative heating to the afterbody, it will be necessary to understand the thermodynamics of the wake. Spectral and total measurements of the radiation emitted at the body's shoulder and in the wake can provide insight into

the thermodynamic state of the wake gas. An experiment designed to obtain these data has been included as part of the experiments aboard the AFE. These data, combined with other experimental data and computational modeling, would allow the accurate prediction of ASTV wake flow and make efficient ASTV design possible.

Acknowledgments

This work was partly supported by NASA Grants NCC2-653 and NCC2-420. The authors are deeply indebted to E. E. Whiting, R. A. Craig, A. Wilhelmi, and C. Sobek for their valuable suggestions and assistance.

References

[1]Walberg, G. D., "A Survey of Aeroassisted Orbit Transfer," *Journal of Spacecraft and Rockets,* Vol. 22, No. 1, 1985, pp. 3–18.

[2]Howe, J. T., "Introductory Aerothermodynamics of Advanced Space Transportation Systems," *Journal of Spacecraft and Rockets,* Vol. 22. No. 1, 1985, pp. 19–26.

[3]Park, C., "A Review of Shock Waves Around Aeroassisted Orbital Transfer Vehicles," NASA TM-86769, June 1985.

[4]National Commission on Space, *Pioneering the Space Frontier,* Bantam, New York, 1986, p. 103.

[5]"National Aeronautical R & D Goals—Agenda for Achievement," Rept., Executive Office of the President, Office of Science and Technology Policy, Washington, DC, 1987.

[6]Nestler, D. E., and Brant, D. N., "Development of an Afterbody Radiative and Convective Heating Code for Outer Planet Probes," AIAA Paper 78-8620, May 1978.

[7]Shieh, P. K., and Gay, A., "Low *L/D* Aerobrake Heat Transfer Test at Mach 10," *Thermal Design of Aeroassist Orbital Transfer Vehicles,* edited by H. F. Nelson, Progress in Astronautics and Aeronautics, AIAA, New York, 1985, pp. 378–394.

[8]Park, C., "Problems of Radiative Base Heating," AIAA Paper 79-0919, May 1979.

[9]Lykoudis, P. S., "A Review of Hypersonic Wake Studies," Memorandum RM-4493-ARPA, May 1965.

[10]Strawa, A. W., Davy, W. C., and Kruse, R., "Measurements in the Wake of Blunt Aerobrakes at 1.8 km/s and 4.9 km/s," *Journal of Spacecraft and Rockets* (to be published).

[11]Canning, T. N., and Page, W. A., "Measurement of Radiation From the Flow Fields of Bodies Flying at Speeds Up to 13.4 Kilometers Per Second," AGARD 68, *High Temperature Aspects of Hypersonic Flow,* edited by W. C. Nelson, London, 1963, pp. 569–582.

[12]Stephenson, J. D., "Measurement of Optical Radiation from the Wake of Ablating Blunt Bodies in Flight at Speeds up to 10 km per second," NASA TN D-2760, April 1965.

[13]Cauchon, D. L., "Project Fire Flight 1 Radiative Heating Experiment," NASA TM X-1222, Oct. 1966.

[14]Shirai, H., and Park, C., "Experimental Studies of Radiative Base Heating of a Jovian Entry Model," *Entry Heating and Thermal Protection,* edited by W.B. Olstad, Vol. 69, Progress in Astronautics and Aeronautics, AIAA, New York, 1980, pp. 148–171.

[15]Shirai, H., and Park, C., "Shock-Tube Studies of Radiative Base Heating of Jovian Probe," *Shock Tubes and Waves: Proceedings of the 12th International Symposium on Shock Tubes and Waves,* The Magnes Press, The Hebrew Univ., Jerusalem, Israel, 1980, pp. 419–428.

[16]Chapman, D. R., Kuehn, D. M., and Larson, H. K., "Investigation of Separated Flows in Supersonic and Subsonic Streams with Emphasis on the Effects of Transition," NACA Rept. R-1356, 1958.

[17]Korst, H. H., "A Theory for Base Pressure in Transonic and Supersonic Flow," *Journal of Applied Mechanics,* Vol. 23, Dec. 1956, pp. 593–600.

[18]Park, C., "Modeling of Radiative Heating in Base Region of Jovian Entry Probe," *Entry Heating and Thermal Protection,* edited by W.B. Olstad, Vol. 69, Progress in Astronautics and Aeronautics, AIAA, New York, 1980, pp. 124–147.

[19]Sambamurthi, J., and Lee, Y., "Aeroassist Flight Experiment Carrier Thermal Environments Data Book," Marshall Space Flight Center, MSFC-DOC-1607, Huntsville, AL, May 1991.

[20]Gnoffo, P. A., Price, J. M., and Braun, R. D., "On the Computation of Near Wake, Aerobrake Flowfields," AIAA Paper 91-1371, June 1991.

[21]Wells, W. L., "Free-Shear Layer Turning Angle in Wake of Aeroassist Flight Experiment (AFE) Vehicle at Incidence in $M = 10$ Air and $M = 6$ CF_4," NASA TM 100479, Nov. 1988.

[22]Gnoffo, P. A., and Greene, F. A., "A Computational Study of the Flowfield Surrounding the Aeroassist Flight Experiment Vehicle," AIAA Paper 87-1575, June 1987.

[23]Li, C. P., and Wey, T. C., "Numerical Simulation of Hypersonic Flow Over an Aeroassist Flight Experiment Vehicle," AIAA Paper 88-2675, June 1988.

[24]Gnoffo, P. A., "A Code Calibration Program in Support of the Aeroassist Flight Experiment," AIAA Paper 89-1673, June 1989.

[25]Palmer, G., "Explicit Thermochemical Nonequilibrium Algorithm Applied to Compute Three-Dimensional AFE Flowfields," *Journal of Spacecraft and Rockets,* Vol. 27, No. 5, 1990, pp. 545–553.

[26]Tam, L. T., and Li, C. P., "Comparisons of Thermochemical Nonequilibrium Viscous Flowfield Predictions for AFE Vehicle," AIAA Paper 90-0141, Jan. 1990.

[27]Park, C., "Assessment of Two-Temperature Kinetic Model for Ionizing Air," AIAA Paper 87-1574, June 1987.

[28]Davies, C., and Venkatapathy, E., "Application of a Solution Adaptive Grid Scheme, SAGE, to Complex Three-Dimensional Flows," AIAA Paper 91-1594, June 1991.

[29]Venkatapathy, E., Palmer, G., and Prabhu, D. K., "AFE Base Flow Calculations," AIAA Paper 91-1372, June 1991.

[30]Park, C., "Nonequilibrium Air Radiation (NEQAIR) Program: User's Manual," NASA TM 86707, July 1985.

[31]Nardone, M., Breene, R. G., Zeldin, S., and Riethof, T. R., "Radiance of Species in High Temperature Air," General Electric, Missile and Space Division, R63SD3, Philadelphia, PA, May 1963.

Michael E. Tauber
Associate Editor